This manuscript has been published in the journal Sensors and Actuators B: Chemical
https://doi.org/10.1016/j.snb.2025.138596

Simultaneous dynamic NO, H_2O, and temperature measurement using an intrapulse laser with MHz time resolution

Denghao Zhu [a, *], Leopold Seifert [a], Sumit Agarwal [a], Bo Shu [a], Ravi Fernandes [a, b], Zhechao Qu [a, *]

a. Department of Physical Chemistry, Physikalisch-Technische Bundesanstalt, Braunschweig, Germany

b. Institute of Internal Combustion Engines, Technische Universität Braunschweig, Braunschweig, Germany

∗ Corresponding authors

E-mail addresses: denghao.zhu@ptb.de (D. Zhu); zhechao.qu@ptb.de (Z. Qu)

Abstract

This study aims at fast and accurate sensing in dynamic conditions using the intrapulse laser technique. Integrated with a shock tube and three other independent lasers, the intrapulse laser was examined for both fundamental and practical applications across varying temperatures and pressures. The spectral regions selected in this study range from 1914 to 1916 cm^{-1}, including both NO and H_2O absorption peaks, enabling simultaneous measurements of NO and H_2O mole fraction as well as temperature using a two-line thermometry. The intrapulse laser operated at a 900 kHz repetition rate with a 200 ns pulse width, achieving a time resolution comparable to the fixed-wavelength method. The chirp rate of the intrapulse laser is 250-400 MHz, providing a spectral resolution of 0.0156-0.0197 cm^{-1}. To correct the rapid passage effect observed under low-pressure conditions, a novel method of symmetrically flipping half of the unaffected spectrum has been proposed and validated. Specific experiments were designed to validate the capability of the intrapulse laser in accurately quantifying NO, H_2O and temperature. The results show that NO and H_2O measurements from the intrapulse laser aligned well with those from an ICL NO laser and a DFB H_2O laser, respectively. Additionally, the temperatures inferred by the intrapulse laser match well with calculations from one-dimensional shock equations. The average relative differences on NO mole fraction, H_2O mole fraction and temperature are 4.5%, 7.0%, and 5.4%, respectively. In an application case, the intrapulse laser successfully captures the dynamic formation process of NO and H_2O and the associated temperature variations during NH_3 oxidation in the shock tube. The results demonstrate good agreement with simulation results from a chemical mechanism. Thus, the intrapulse laser is a powerful technique that enables simultaneous measurements of multiple species and

temperature in dynamic environments, combining the calibration-free advantage of the scanned-wavelength method with the high time resolution of the fixed-wavelength method.

Keywords: intrapulse laser, rapid passage effect, mole fraction, temperature, shock tube, laser absorption spectroscopy, dynamic measurement

1. Introduction

Quantifying dynamic quantities such as speciation mole fraction and temperature is crucial in various scientific and industrial applications, including environmental monitoring, space exploration, chemical reactions, technical thermodynamics and safety control, which requires fast and accurate sensing techniques. Laser absorption spectroscopy (LAS) is an *in-situ* and non-invasive measurement method with high time-resolution and selectivity [1,2]. It has been well-established and developed for air pollution monitoring, agricultural, industrial, and automotive emissions detection, medical and combustion diagnostics [3-8]. With the development of quantum cascade lasers (QCL) that operate based on intersubband transitions within the conduction band of a semiconductor material, longer wavelengths with narrow linewidth and high-power output can be achieved, making QCL an ideal light source for mid-infrared (MIR) laser spectroscopic gas sensing [9,10]. Generally, QCL operates in continuous-wave (CW) mode. To enhance time resolution for dynamic measurements, either a fixed-wavelength method or a high frequency tunning can be applied. The fixed-wavelength method is relatively simple but provides limited spectral information and requires frequent calibration and maintenance to ensure measurement accuracy. This method also suffers from limited applicability, sensitivity, and flexibility, and is susceptible to interference from other substances. Conversely, the scanned-wavelength method can overcome these obstacles by providing calibration-free results. However, the tunning range of a CW-QCL decreases exponentially as the scan frequency increases. Our previous studies have shown that the tunning range is limited to 0.3 cm^{-1} when the scan frequency reaches 40 kHz for a QCL NH_3 laser [11]. This limitation makes it challenging to further enhance the scan frequency to meet the requirements for higher time resolution measurement.

The intrapulse laser technique, operating a QCL in pulse mode rather than CW mode, combines the advantages of a wide tuning range and high time resolution. The basic principle of intrapulse spectroscopy involves rapid frequency downchirp by applying a step rise in injection current, modulated by a rectangular pulse train. The tuning range of an intrapulse laser can be over 10 cm^{-1} with a repetition rate over megahertz and a pulse width of hundreds of nanoseconds. This performance is comparable to the time resolution of the fixed-wavelength method but providing calibration-free results. The chirp rate of an intrapulse laser typically reaches hundreds of megahertz per nanosecond, with a typical spectral resolution of around 0.02 cm^{-1}.

Up to now, there are limited studies on intrapulse laser. Normand et al. [12] coupled an intrapulse laser with a multiple-pass absorption cell to detect 1,1-difluoroethylene, achieving a sensitivity of 500 parts per billion (ppb). Manne et al. [13] compared the inter- and intrapulse techniques for ammonia and ethylene quantification in a Herriot cell with 150 m optical path length. They achieved a detection limit of 3 ppb for ammonia and 5 ppb for ethylene within 10 seconds averaging time. Similarly, Nwaboh et al. [14] and Jacquemin et al. [15] used intrapulse lasers to measure CO and CO_2 concentration in gas cells, respectively. Simultaneous CO_2 and temperature measurements were conducted by Herklotz et al. [16,17] in a gas cell using a single intrapulse laser. Their results showed good agreement with static temperature measurements ranging from 20-40°C, as compared with a Pt100 sensor. Another application by Hübner et al. [18] was to use an intrapulse laser for temperature measurement in a pulsed dc air plasma.

The aforementioned investigations were mainly focused on static measurements with lower requirements for time resolution. Consequently, the intrapulse lasers operated at a repetition rate of less than 50 kHz. However, fast processes, such as combustion, demand higher time resolution. Aamir Farooq's group utilized intrapulse lasers for high-speed combustion diagnostics both in a shock tube and a rapid compression machine. They measured H_2O mole fraction and temperature in the shock tube at a repetition rate of 250 kHz [19]. The chirp rate was between 20 to 60 MHz/ns and the spectral resolution was 0.013 to 0.021 cm^{-1} for their system. They also succeeded to infer temperature using two intrapulse lasers at a repetition rate of 100 kHz in the rapid compression machine [20,21]. Geoffrey Duxbury' group conducted continuous fundamental studies on the intrapulse laser over ten years, focusing particularly on the unique phenomenon known as the rapid passage effect. This effect occurs at low pressures and high scan frequencies when the laser's sweep rate through a Doppler broadened absorption line is much faster than the collisional relaxation time, and the power density of the linearly polarized laser radiation is sufficient to cause optical pumping. A numerical model was developed to simulate this effect [12, 22-25]. Except for theoretical study, they also applied the intrapulse laser for real-time exhaust gases measurement of an aero gas turbine engine [26]. The rapid passage effect was also reported by Helden et al. [27] who observed this phenomenon in low-pressure plasma experiments and characterized its impact on CH_4 number density. In this study, we also observed the rapid passage effect at low pressure conditions. More details will be introduced later.

Based on the above literature reviews, although the investigations on the intrapulse laser are scarce, it has proven to be a powerful technique, combining the advantages of a wide tunning range and high time resolution. In this study, we utilized the shock tube as a reactor to create a

dynamic environment to test the performance of the intrapulse laser. Unlike previous studies that focus solely on the high-pressure and high-temperature environment after the reflected shock wave, our research encompasses the entire dynamic process of shock wave propagation. This approach covers a wide pressure range from millibar to bar and a temperature span from room temperature to several thousand kelvins. An intrapulse, along with three other lasers, were coupled with the shock tube. Our approach aims to 'killing three birds with one stone' by using a single intrapulse laser for simultaneous dynamic measurements of NO, H_2O and temperature. The repetition rate of the intrapulse laser is up to MHz, which is relatively higher than previous studies. The structure of this paper would be as follows: 1) Introduction to the methodology and experimental setup; 2) Illustration of spectroscopic characteristics of the intrapulse laser; 3) Individual validation the capability of measuring NO mole fraction, H_2O mole fraction, and temperature by the intrapulse laser; 4) Demonstration of a simultaneous dynamic NO, H_2O, and temperature measurement case using a single intrapulse laser.

2. Methodology

To get the absolute mole fraction as well as temperature, the widely used technique, laser absorption spectroscopy (LAS), has been employed. For LAS, the transmitted intensity $I_t(v)$ of a monochromatic laser source through a gaseous sample is given by Beer-Lambert law [28]:

$$I_t(v) = E(t) + I_0(v) \cdot \eta(t) \cdot exp[-\alpha(v)] \quad (1)$$

with the background emission $E(t)$ at time t, initial laser intensity $I_0(v)$, absorbance $\alpha(v)$, and the broadband transmission losses $\eta(t)$ which are synchronously derived from the individual raw signals and absorption profiles. The exponential term can be computed using the following equation:

$$\alpha(v) = -\ln\left(\frac{I_t(v)-E(t)}{I_0(v)\cdot\eta(t)}\right) \quad (2)$$

The Voigt function can be used to model the line shape of the absorbance spectrum in Eq. (2), which considers the combined effects of Doppler and collisional broadening on the spectral line. These effects are characterized by the Doppler broadening full width at half maximum (FWHM), Δv_D, and the collisional-broadening FWHM, Δv_L, given by

$$\Delta v_D = v_0\sqrt{\frac{8k_B T \ln 2}{Mc^2}} \quad (3)$$

$$\Delta v_L = 2 \cdot p \cdot \sum_i (x_i \cdot \gamma_{i-j}(T_0) \cdot (\frac{T_0}{T})^{n_{i-j}}) \quad (4)$$

where k_B is the Boltzmann constant with a value of 1.380649E-23 J/K, T is the temperature, M is the molecular mass of the absorbing species, c is the speed of light, p is the total pressure, x_i

is the mole fraction of the *i*th specie in the mixture, $\gamma_{i\text{-}j}(T_0)$ is the collisional broadening coefficients of the *i*th specie to the *j*th specie at T_0=296 K. $n_{i\text{-}j}$ is the temperature dependence coefficient of the collisional broadening for the *i*th specie to the *j*th specie.

By integrating the absorbance spectrum, the absolute mole fraction can be obtained by the following equation:

$$A=\int \alpha(\nu)=\frac{S(T)\cdot p\cdot L\cdot x}{k_{\mathrm{B}}\cdot T} \tag{5}$$

Where A is the integrated area of the absorbance, $S(T)$ is the absorption line intensity at gas temperature T.

For the scanned-wavelength absorption technique, the ratio of integrated area is directly proportional to the line intensity ratio:

$$\frac{S(T)_1}{S(T)_2}=\frac{A_1}{A_2} \tag{6}$$

Hence, the temperature can be inferred based on the two-line thermometry.

3. Experimental setup

Shock tube serves as a versatile tool utilized in various research disciplines such as aerodynamics, physics, and chemical kinetics. It enables the generation of a highly dynamic environment, starting from millibar pressure and room temperature before the incident shock wave, to high temperatures exceeding thousand kelvin and megapascal pressures behind the reflected shock wave, with test durations ranging from microseconds to milliseconds. This unique capability is leveraged for dynamic quantity measurements using laser absorption spectroscopy. Figure 1 depicted the schematic of the experimental setup, including shock tube and laser diagnostic parts. A detailed introduction to the shock tube at the Physikalisch-Technische Bundesanstalt (PTB) can be found in Ref. [29]. Here, only a brief introduction is given.

The shock tube consists of a 3.5-meter driver section and a 4.5-meter driven section separated by aluminum diaphragms, with an overall inner diameter of 70 mm. Five pressure sensors (603CAB, Kistler) combined with charge amplifiers (5018A, Kistler) were utilized for pressure measurement and shock velocity calculation. The pressure and temperature during the shock front propagation were calculated using one-dimensional shock equations. The mixtures were prepared in a 50 L stainless steel tank. Before preparing the mixtures, the mixing tank was vacuumed to a pressure of 1×10^{-7} mbar. When starting to prepare the mixture, a small amount of target gas first flushes the pipes twice to clean up residual gas. The mixtures were stirred by a magnetic stirrer (Büchiglasuster cyclone 300 ac) for at least two hours to ensure homogeneity.

For laser diagnostics, two opposite Zinc Selenide (ZnSe) windows were installed at the same plane as the fourth pressure sensor. In total four lasers were coupled with the shock tube, including one intrapulse laser, two independent NO and H_2O lasers to validate the NO and H_2O mole fraction, and one NH_3 laser to quantify NH_3 mole fraction considering its strong adsorption effect. Specifically, the intrapulse laser is a single mode quantum cascade laser (QCL, mirSense) centered at 1915.7 cm^{-1} with a tuning range from 1913 to 1923 cm^{-1}. The repetition rate ranges from 3 kHz to 1MHz, and the pulse width ranges from 10 ns to 300 ns. In this study, the repetition rate is fixed at 900 kHz with a fixed pulse width of 200 ns. With such high repetition rate, the period of one pulse is only 1.11 μs, which is the same level as a fixed-wavelength method. The NO laser is a continuous-wave distributed-feedback interband cascade laser (CW-DFB-ICL, Nanoplus) with the same center wavenumber as intrapulse laser. The ICL NO laser is driven by a modular laser diode controller (LDC-3900, ILX Lightwave) and modulated by a triangle-shaped ramp at a scan frequency of 280 Hz supplied by a function generator (33500B, KEYSIGHT). The near-infrared (NIR) H_2O laser is a DFB diode laser (NEL Laser Diodes) in a butterfly-type with a wide tunning range of 6849-7353 cm^{-1}. It is driven by the same modular laser diode controller used for ICL NO laser. The center wavelength of this DFB laser was tunned at 7154.35 cm^{-1} modulated by a triangle-shaped ramp at a scan frequency of 20 kHz. For NH_3 quantification, a continuous-wave distributed-feedback quantum cascade laser (CW-DFB-QCL, Alpes Lasers) centered at 1084.6 cm^{-1} was used. It can be tuned from 1083 to 1089 cm^{-1} through a QCL driver (ITC4005QCL, Thorlabs). The laser current was modulated by a triangle-shaped ramp at a scan frequency of 40 kHz.

Four lasers were well aligned and collimated into a concave mirror (CM508-200-M01, focal length: 200 mm, Thorlabs) and went through the optical windows with a path length of 7 cm. The laser beams were separated by beam splitters and focused onto four different photodetectors (UHSM-10.6 for intrapulse laser, PVI-4TE-5 for ICL NO laser, PVI-4TE-10.6 for QCL NH_3 laser, VIGO; PDA20CS2 for DFB H_2O laser, Thorlabs). Besides, specific bandpass filters (CWL=5219 nm, BW=30 nm, Laser Components; CWL=1400 nm, FWHM=12 nm, Thorlabs; CWL=9000 nm, FWHM=500 nm, Thorlabs) were placed in front of the photodetectors to discriminate the signal against the background emission *E(t)* in Equation (1), e.g., thermal emission from the shock-heated gases.

Before starting the measurements, the dynamic laser tuning was determined using two etalons. One is a Germanium etalon (length 76.244 mm) for intrapulse laser, ICL NO laser and QCL NH_3 laser in MIR regions. The other one is a ZnSe etalon (length 102.8 mm) for H_2O laser in NIR regions. The result of the etalon measurement was used to convert the x-axis of the

measured spectra from the time to the wavenumbers domain. To match the ultra-rapid repetition rate of the intrapulse laser, a high-speed oscilloscope (MSO56B, Tektronix) with a sample rate of 6.25 GS/s was used. The rest three laser signals as well as the pressure signals were acquired by a data acquisition card (16-bit 80 MS/s, M2p.5943-x4, Spectrum Instrumentation) and visualized by the software (SBench6-Pro).

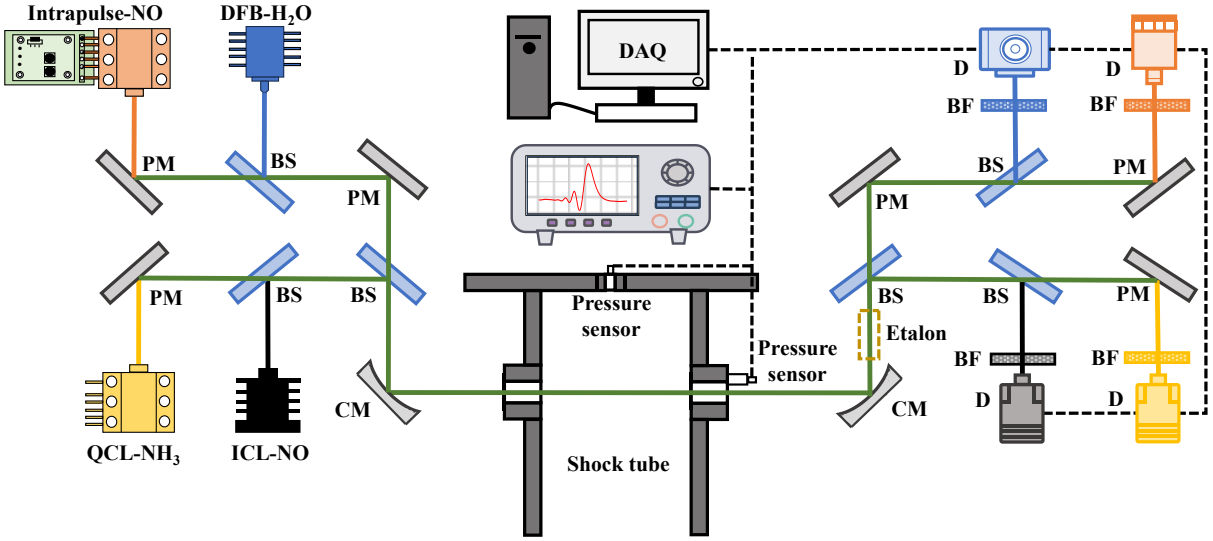

Figure 1(a). Schematic of the experimental setup (DFB: Distributed Feeback; QCL: Quantum Cascade Laser; ICL: Interband Cascade Laser; D: Detector; DAQ: Data Acquisition; PM: Plane Mirror; BS: Beam Splitter; CM: Concave Mirror; BF: Bandpass Filter)

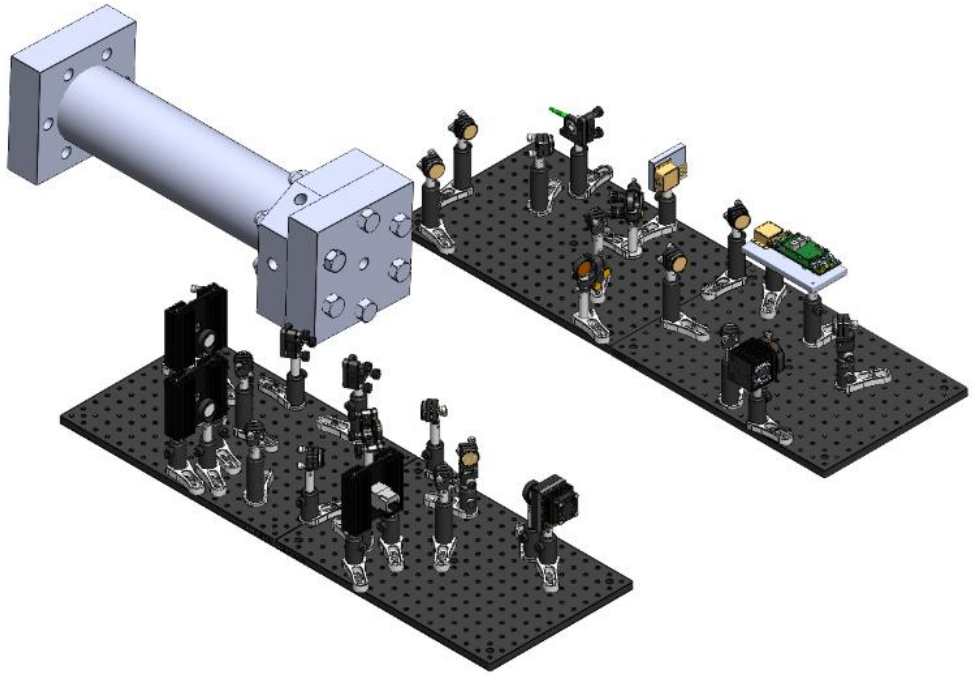

(b). 3D view of experimental setup

4. Spectroscopic fundamentals

4.1 Line selection and typical spectrum

The aim of this study is to use a single intrapulse laser for simultaneous quantification of NO and H_2O, along with temperature measurement using two-line thermometry. In our previous studies, the NO absorption lines centered at 1914.99 cm^{-1} and 1915.76 cm^{-1} have been investigated. We measured the broadening coefficients of these two absorption peaks at room temperature and pressure [30] and quantified NO mole fraction during combustion processes using a fixed-wavelength method at 1915.76 cm^{-1} [29]. Building upon this knowledge, the two NO absorption peaks are employed here for NO quantification and temperature calculation. Additionally, between these two NO absorption peaks, strong H_2O absorption peaks appear at high temperatures. Figure 2 illustrates simulated absorption spectra in a 1% NO/1% H_2O/Air (buffer gas) mixture based on HITRAN database [31], with an optical length of 7 cm at two different conditions: low pressure and room temperature (0.01 bar, 295 K); high pressure and high temperature (1bar, 2000 K). At 0.01 bar and 295 K, there are two distinct peaks around 1914.99 cm^{-1} and one peak at 1915.76 cm^{-1}, with negligible H_2O absorption. At 1bar and 2000 K, pressure broadening causes the two NO peaks to merge into one peak centered around 1914.99 cm^{-1}. Meantime, the absorbance of both NO absorption peaks decrease because of reduced line intensities at higher temperatures. Notably, two prominent H_2O absorption peaks at 1915.19 cm^{-1} and 1915.27 cm^{-1} are clearly observable and will be used to quantify H_2O mole fraction at high temperatures. Additionally, simulations indicate that interferences from other common species such as carbon monoxide (CO) and carbon dioxide (CO_2) are negligible. Therefore, the chosen spectral region effectively meets the requirements for simultaneous measurement of NO, H_2O, and temperature.

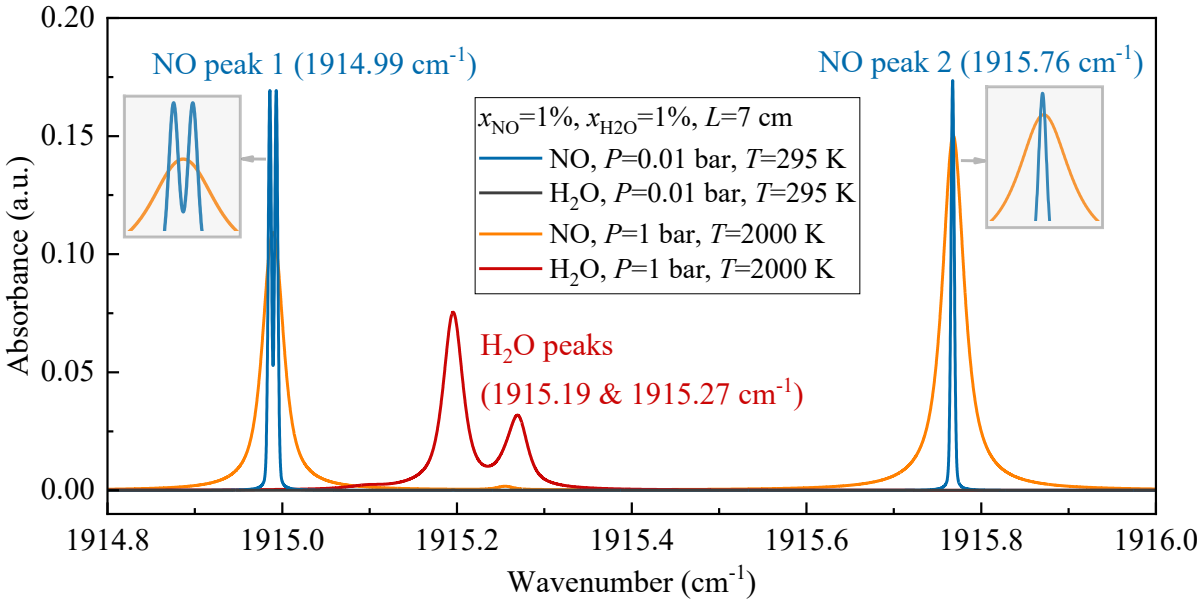

Figure 2. Simulation of the investigated spectra at different conditions

Figure 3(a) shows the measured pressure and raw intrapulse laser signal of 2% NO/98% Ar mixture in the shock tube. The pressure signal exhibits two distinct sharp rises, indicating the arrival of the incident shock wave and the reflected shock wave. The thermodynamic status before the incident shock wave is represented by (T_1, P_1) which is 0.04 bar and 295 K for this case. The mixture was heated by the incident shock wave to the thermodynamic status of (T_2, P_2), yielding a pressure of 0.38 bar and a temperature of 953 K. Then, the pressure and temperature of the mixture was further enhanced to the status of (T_5, P_5) at 1.58 bar and 1817 K by the reflected shock wave.

In the intrapulse laser signal shown in Figure 3(a), there are two interferences marked by dashed line boxes. They are caused by the schlieren effect when the incident and reflected shock fronts pass by the optical window, respectively. The ultra-rapid repetition rate of the intrapulse laser enables recording of over tens of scans within a short time duration of (T_2, P_2). This capability allows for full utilization of the entire dynamic process during shock propagation. Two continuous intrapulse laser signals at (T_2, P_2) are zoomed in for a better view. Further, Figure 3(b) shows a typical reference laser signal I_0, transmitted signal I_t, and absorbance in a single pulse. The transmitted signal aligns well with the reference signal and two absorption peaks of NO are clearly identifiable. These peaks are converted into absorbance using Eq. (1). Unlike a common symmetrical spectrum, the absorbance exhibits an ‘oscillation’ structure, known as the rapid passage effect. This effect often occurs at low pressures and high scan frequencies. It arises because the sweep rate of the laser through a Doppler broadened absorption line is much faster than the collisional relaxation time, and when the power density of the linearly

polarized laser radiation is sufficient to cause optical pumping [23]. Further discussions on this phenomenon will be provided below.

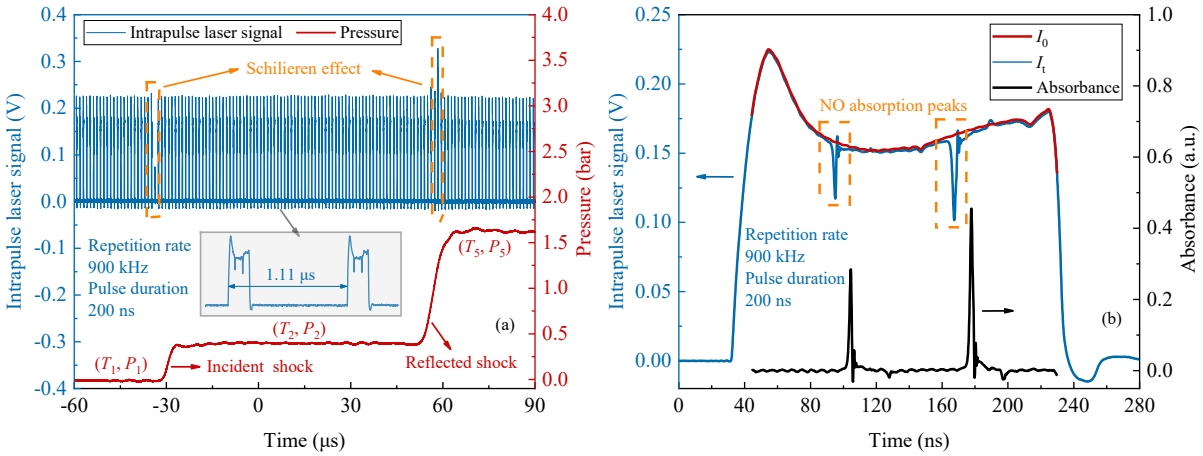

Figure 3. (a) Dynamic pressure and intrapulse laser signal measured in the shock tube at 900 kHz; (b) Reference signal, transmitted signal, and absorbance in a single pulse at 900 kHz

4.2 Chirp rate and spectral resolution

The principle of an intrapulse laser is rendered through rapid frequency downchirp by applying a step rise in injection current. This nonlinear tuning can be depicted through the etalon signal illustrated in Figure 4, where there is an increased separation of the etalon fringes over time. In the Etalon signal, over 100 peaks can be observed within in a single pulse to convert the laser signal from time domain to frequency domain. The Free Spectra Range (FSR) of the Etalon is 0.0163 cm^{-1} at the wavenumber of 1915.7 cm^{-1}. Based on the etalon signal, the chirp rate dv/dt can be calculated ranging from 250 to 400 MHz/ns. For intrapulse lasers, the spectral resolution Δv_{res} is not determined by the effective line width but by the chirp rate of the laser and the time resolution of the detection system [22]. It can be calculated using Eq. (7):

$$\Delta v_{res} = \sqrt{C \cdot dv/dt} \tag{7}$$

Here C is a constant depending on the detection bandwidth. For a rectangular time window, C=0.886 and for a Gaussian window C=0.441 [22]. For the intrapulse laser in this study, it is a rectangular window function as can be seen from Figure 4. The spectral resolution Δv_{res} decreases from 0.0197 cm^{-1} to 0.0156 cm^{-1} with the decrease of chirp rate.

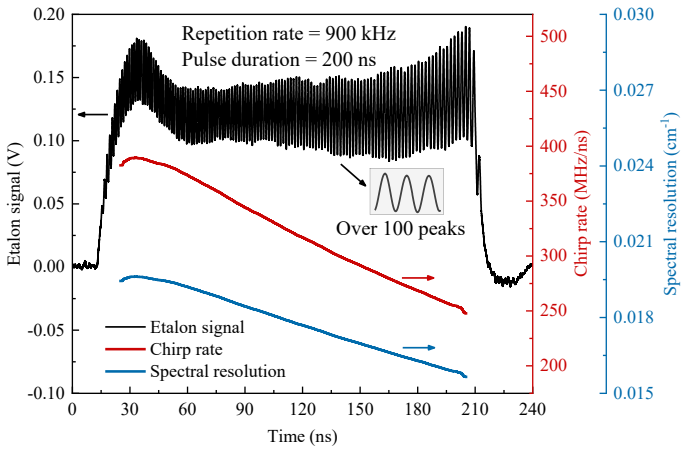

Figure 4. Etalon signal, chirp rate and spectral resolution of a single pulse at 900 kHz

Due to the spectral resolution, the spectrum measured by the intrapulse laser is considerable broadened. Figure 5 compares the spectra of NO centered at 1915.76 cm^{-1} measured using an ICL laser at 280 Hz and an intrapulse laser at 900 kHz. The spectrum measured by high spectral resolution ICL laser (laser line width < 1-2 MHz) is sharper and narrower, whereas the spectrum obtained by the intrapulse laser is broader with low spectral resolution. By using the high-resolution spectrum measured by the ICL laser and the one measured by intrapulse laser, the instrument function of the intrapulse laser spectrometer can be obtained. The high-resolution spectrum is convolved with a Gaussian function, then fitted to the low-resolution spectrum using Least Squares Method. By applying such best spectrum fitting, the width of Gaussian function can be obtained. The black line in Figure 5 represents the convolved spectrum, which effectively reproduces the overall line shape observed with the intrapulse laser. The width of the best-fit Gaussian function is 0.017 cm^{-1}, consistent with the spectral resolution at a wavenumber of 1915.76 cm^{-1} calculated from Eq. (7). This finding strongly underscores the validity and significance of spectral resolution in intrapulse spectroscopy, akin to the instrument function in Fourier-transform infrared spectroscopy (FTIR).

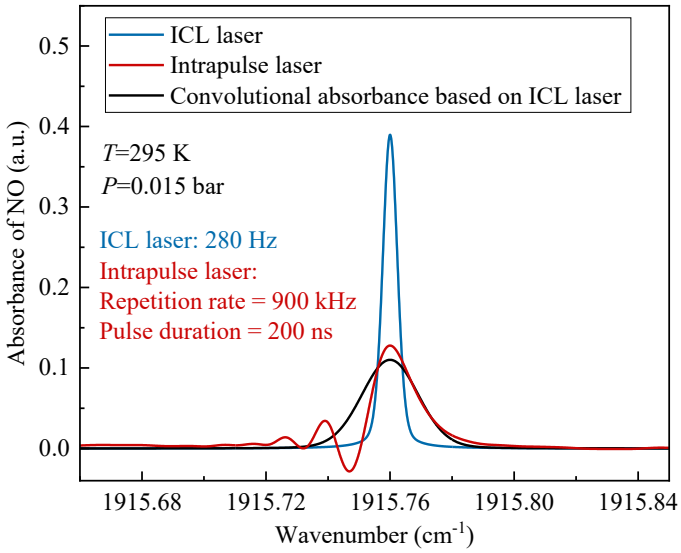

Figure 5. Spectrum of NO measured by ICL laser at 280 Hz, convolutional spectrum based on ICL laser, and NO absorbance measured by intrapulse laser at 900 kHz

4.3 Rapid passage effect

As previously discussed, the oscillatory structure known as the rapid passage effect is observed in the spectrum of an intrapulse laser. It is a delayed switch from absorption to emission, leading to the generation of a large, narrow, transient gain signal [24]. This phenomenon is particularly evident at low pressures due to two primary reasons: 1) Reduced collisional broadening: at low pressures, the frequency of collisions between molecules is significantly reduced. Collisions tend to broaden the spectral lines and introduce dephasing, which disrupts the coherent interaction between the laser light and the medium. With fewer collisions, the spectral lines are narrower, and the coherence time is longer, allowing the rapid passage effect to be more prominent; 2) Enhanced quantum interference: the rapid passage effect involves quantum interference between different energy states of the atoms or molecules. At low pressure, the reduced collisional interactions mean that quantum coherence can be maintained over longer timescales, enhancing the interference effects that are central to the rapid passage phenomenon. In short, at low pressure conditions, the interactions between the laser light and the medium can occur with minimal disturbances from collisions and broadening effects, allowing the coherent and rapid transitions between energy states to be observed more clearly. This observation aligns with experimental findings. Figure 6 shows the absorbance spectra measured at different pressures, corresponding to different stages during shock propagation. As pressure increases, the rapid passage effect becomes significantly suppressed and eventually disappears at higher pressures. This observation underscores the pressure-dependent nature of the rapid passage phenomenon in intrapulse spectroscopy.

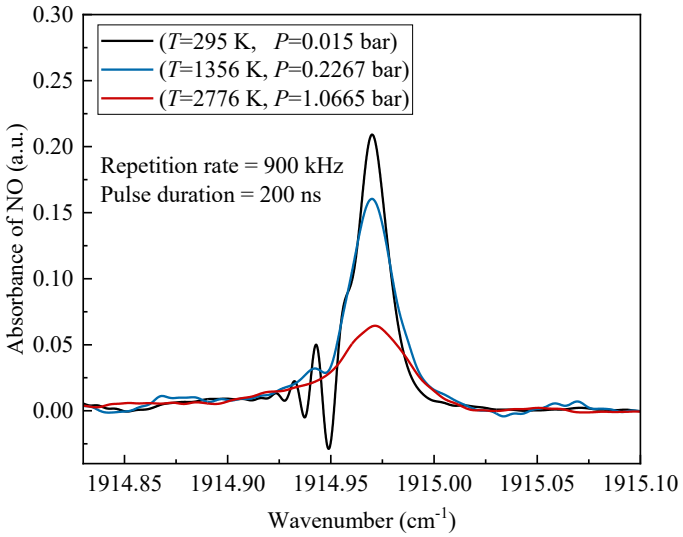

Figure 6. Absorbance of NO measured by intrapulse laser at different pressures and temperatures in the shock tube

Regarding the rapid passage effect, Duxbury et al. [22-25] have made significant efforts to model it, drawing parallels from similar effects observed in frequency-swept nuclear magnetic resonance (NMR). In this study, we propose a simple and practical method to mitigate the impact of the rapid passage effect on mole fraction calculations. From observations of the rapid passage effect, it typically begins smoothly and exhibits oscillations primarily at the "wings" of the spectrum where the chirp rate decreases. Given that, we propose a method to symmetrically flip half of the spectrum that remains unaffected by the rapid passage effect. Figure 7 provides an example of this approach, where the flipped absorbance is shown along with a Voigt fit, yielding a standard deviation of residual σ=8.5×10^{-4}. This method intuitively reflects the structure of the rapid passage effect by comparing the spectrum before and after applying the flip operation. The efficacy and validity of this proposed method will be further detailed and discussed in the subsequent chapter.

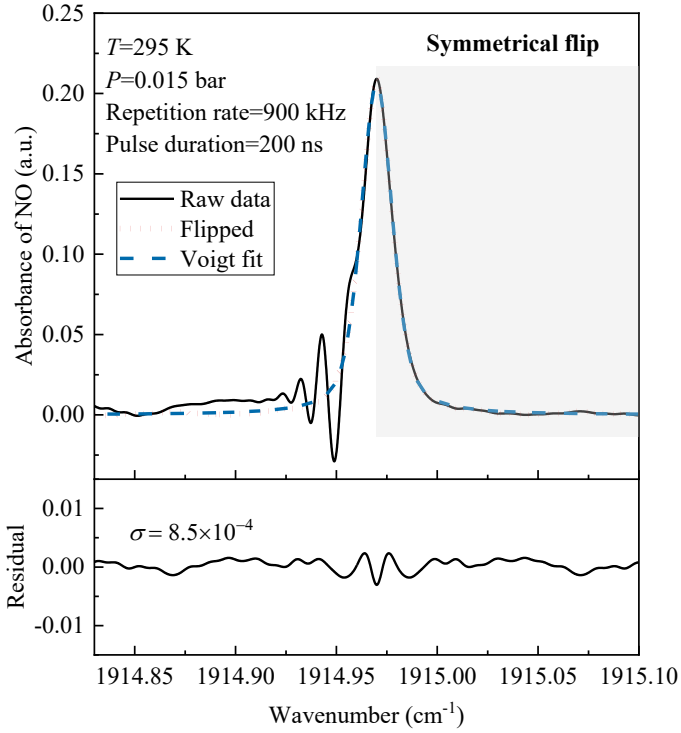

Figure 7. The measured NO spectrum with 'oscillatory structure' - rapid passage effect, symmetrical flipped spectrum of the raw spectrum, and Voigt fit of the flipped spectrum

5. Validation

In this chapter, the shock tube is used as a versatile reactor to generate dynamic conditions spanning from (T_1, P_1) to (T_5, P_5). Using the intrapulse laser, we aim to measure speciation mole fractions and infer temperatures across the entire dynamic process. These measurements will be compared against results obtained from independent lasers or simulations to validate their accuracy and reliability. More details will be introduced below.

5.1 NO mole fraction

Firstly, we target the validation of the NO mole fraction. Shock tube experiments were conducted over a pressure range of 0.01 to 1.49 bar and a temperature range of 295 to 2775 K using a mixture of 2% NO and 98% Ar. An ICL NO laser, swept at a scan frequency of 280 Hz, served as the benchmark for determining the NO mole fraction before the incident shock (T_1, P_1). The intrapulse laser measured the dynamic NO mole fraction throughout the entire shock propagation at a repetition rate of 900 kHz and a pulse width of 200 ns. As shown in Figure 3, two NO peaks centered at 1914.99 cm^{-1} and 1915.76 cm^{-1} were obtained within one scan by the intrapulse laser. Both peaks can be utilized to determine the NO mole fraction; however, for illustration purposes, we will focus on the first peak centered at 1914.99 cm^{-1}.

This peak serves as a representative example to demonstrate the intrapulse laser's capability in capturing dynamic NO mole fraction measurements during the shock tube experiments.

Figure 8 shows the NO mole fraction measured by intrapulse laser w/o flipped absorbance and compared to the results by an independent ICL laser. The procedure to calculate mole fraction is consistent for both the ICL laser and the intrapulse laser. Firstly, the raw absorbances measured at (T_1, P_1) are averaged to smooth the spectrum for better signal-to-noise ratio. Due to the ultra-fast repetition rate of the intrapulse laser, over 300 spectra can be recorded at (T_1, P_1) within just 3 milliseconds. After averaging the spectra, a Voigt fit is applied to the smoothed spectrum. The mole fraction is then calculated according to Eq. (5).

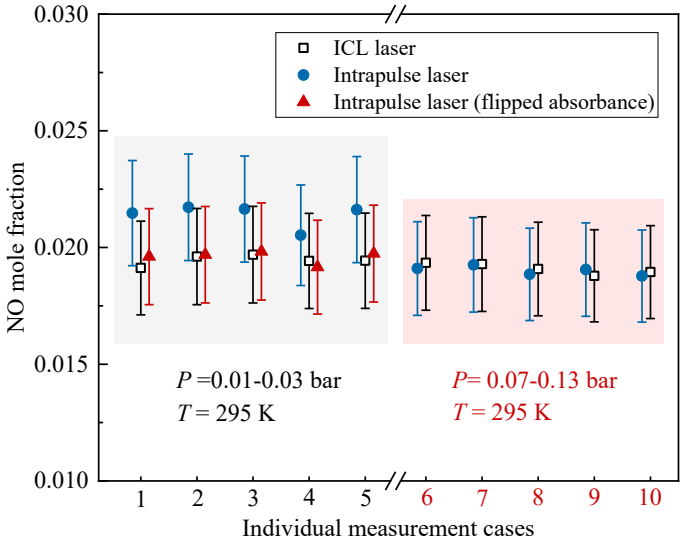

Figure 8. NO mole fraction measured by intrapulse laser w/o flipped absorbance, and compared to the results by an independent ICL laser

In total ten individual measurements were performed across two pressure groups: 0.01-0.03 bar and 0.07-0.13 bar. The lower pressure group (0.01-0.03 bar) exhibited a strong impact from the rapid passage effect, leading to a relatively higher NO mole fraction measured by the intrapulse laser compared to the ICL laser results. However, after applying the flipped absorbance, the NO mole fraction aligned much more closely with the values obtained by the ICL laser. The relative difference between the NO mole fraction measured by the intrapulse laser and ICL laser reduces from 10% to 1.3%. This result validates our proposed method for mitigating the impact of the rapid passage effect on mole fraction calculations. Compared to the theoretical modelling of the rapid passage effect, this method seems simpler and more practical for real-world applications. For the second group measurements conducted at higher pressure (0.07-0.13 bar), although rapid passage effects were still observable in the spectrum,

their impact on NO mole fraction was negligible. These findings underscore the effectiveness of our absorbance flipping method in correcting for the rapid passage effect.

Uncertainty analysis is always important for reliable results. The standard uncertainty $u(x)$ can be calculated following the 'Guide to the Expression of Uncertainty in Measurement (GUM)', which is the positive squared root of the combined variances given by [32]:

$$u(x) = \sqrt{\sum_{i=1}^{N}(\frac{\partial f}{\partial Y_i} \cdot u(Y_i))^2} \quad (8)$$

where $u(Y_i)$ is the uncertainty of the ith quantity. The coverage factor k is given as 1 in this study.

From Eq. (5), there are in total six quantities, including Boltzmann constant k_B, temperature T, absorbance area A, line intensity $S(T)$, optical pathlength L and pressure p. k_B is the Boltzmann constant with a value of 1.380649E-23 J/K. From our previous study [11], the uncertainties of T_1, P_1 and L are 0.17%, 0.15% and 1.1%, respectively. The uncertainty of absorbance area is 3% in this study. The line intensity is adopted from the HITRAN database with an uncertainty of 10% [31]. Hence, the uncertainty of NO mole fraction is calculated to be 10.5%. From the uncertainty budget, 90.9% of the uncertainty contribution arises from the uncertainty in line intensity. To address this, our future work will focus on measuring the line intensity of these two NO peaks to reduce this uncertainty.

The second part focus on validating the dynamic NO mole fraction measured by the intrapulse laser. Five individual measurements were performed in the shock tube, using an independent ICL NO laser as a benchmark. The initial pressures of five shots ranged between 0.01 and 0.03 bar. This corresponds to a pressure of 0.23-0.34 bar and temperature of 965-1356 K after incident shock wave (T_2, P_2), and a pressure of 1.07-1.49 bar and temperature of 1845-2775 K after reflected shock wave (T_5, P_5). Using the same procedure as introduced previously, the dynamic NO mole fraction measured by intrapulse laser at different stages was calculated, as shown in Figure 9. The uncertainties in NO mole fraction at (T_2, P_2) and (T_5, P_5) are 11%, slightly higher than those at (T_1, P_1) due to higher uncertainties in temperatures and pressures. From Figure 9, when accounting for uncertainties, there is a good match between the dynamic NO mole fraction measured by intrapulse laser and the results from the independent ICL laser. The average relative difference between the NO mole fraction measured by the intrapulse laser and ICL NO laser is 4.5%. This result validates the capability of the intrapulse laser for dynamic NO mole fraction measurement.

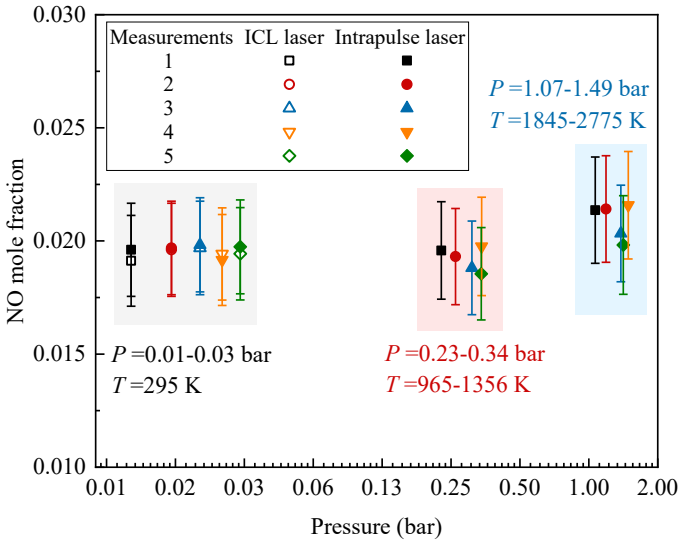

Figure 9. Dynamic NO mole fraction measured by intrapulse laser at different temperatures and pressures in the shock tube, and compared to the results by an independent ICL laser

5.2 H_2O mole fraction

The H_2O mole fraction was measured by the intrapulse laser using the two absorption peaks centered at 1915.19 cm^{-1} and 1915.27 cm^{-1}. An independent DFB H_2O laser centered at 7154.35 cm^{-1} was used as a benchmark for validation. Given a relatively weaker line intensity of these H_2O absorption lines, a mixture of 20% H_2O/ 80% Ar was used for the shock tube experiments. Furthermore, since these three H_2O absorption lines are 'hot' lines, they can only be detected at high temperatures. Figure 10 (a) shows an exemplary reference signal, transmitted signal and absorbance of H_2O measured in a single pulse at a temperature of 1900 K and 1.39 bar. Very distinct absorption peaks can be observed. Figure 10(b) shows an example of a Voigt fit for the absorbance spectrum, which can accurately capture the raw absorbance, with a standard deviation of the residual being 6.6×10^{-3}.

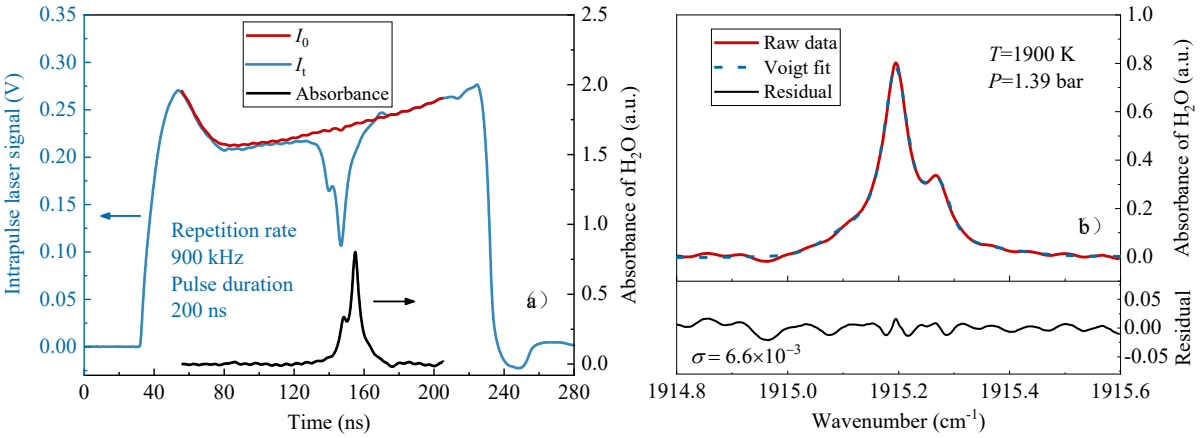

Figure 10. (a) Reference signal, transmitted signal, and absorbance of H_2O in a single pulse at 900 kHz; (b) Raw absorbance and Voigt fit of the absorbance at 1900 K and 1.39 bar

Similar to the NO mole fraction validation experiments, a total of five individual measurements were performed in the shock tube. The initial pressure before the incident shock wave ranges from 0.15-0.4 bar, corresponding to a pressure of 0.21-0.36 bar and a temperature of 842-1168 K at (T_2, P_2), and a pressure of 1.04-1.51 bar and a temperature of 1497-2200 K at (T_5, P_5). The DFB H_2O laser operated at 20 kHz. Figure 11 compares the H_2O mole fraction measurements obtained using the intrapulse laser and the DFB H_2O laser. Note that due to adsorption effect of water vapor, there are some H_2O losses. Therefore, the H_2O mole fraction for each shot is lower than the ideal mole fraction of 20%. Similar phenomenon has also been observed in our previous studies for both water vapor and NH_3 [11].

The uncertainty of the H_2O mole fraction measured by the DFB laser is 10%, while the uncertainty for the intrapulse laser measurements is relatively smaller, which is 3.9% at (T_2, P_2) and 4.5% at (T_5, P_5). This is because the uncertainty of the two absorption peaks centered at 1915.19 cm^{-1} and 1915.27 cm^{-1} is only 2% [31]. As shown in Figure 11, when taking uncertainties into account, the H_2O mole fraction measured by both lasers exhibit satisfactory agreement. The average relative difference between the H_2O mole fraction measured by the intrapulse laser and DFB H_2O laser is 7.0%. Therefore, the capability of using the intrapulse laser for dynamic H_2O quantification is validated.

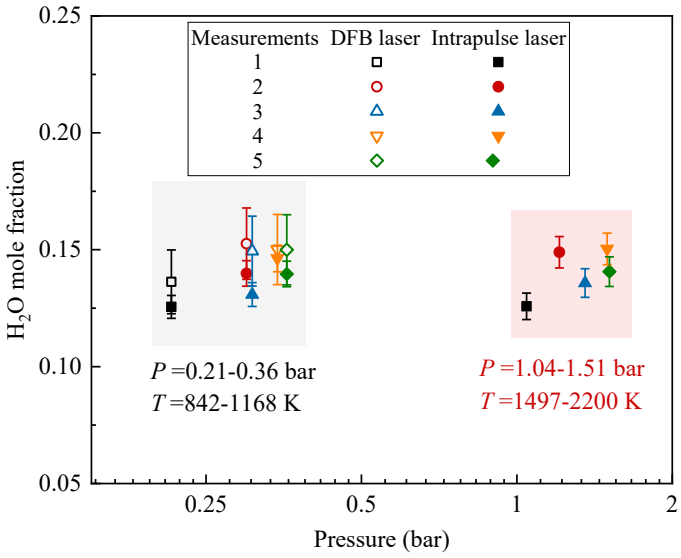

Figure 11. Dynamic H_2O mole fraction measured by intrapulse laser at different temperatures and pressures, and compared to the results by an independent DFB laser

5.3 Temperature

This session validates the capability of inferring dynamic temperature using an intrapulse laser with two-line thermometry. Figure 12(a) presents simulations of line intensity for two NO absorption peaks at 1914.99 cm^{-1} and 1915.76 cm^{-1} from 295-3000 K. Both lines have strong

line intensity over wide temperature ranges, as previously validated. For the absorption line at 1914.99 cm^{-1}, the line intensity decreases monotonically with the increase of temperature. Another line at 1915.76 cm^{-1} reaches its peak intensity at around 450 K and then decreases. For the scanned-wavelength absorption technique, the ratio of integrated area is directly proportional to the line intensity ratio. Figure 12(b) shows the line intensity ratio of line pair 1914.99 cm^{-1}/1915.76 cm^{-1} and corresponding temperature sensitivity. Here the sensitivity is defined as the first derivative of the line intensity ratio versus temperature. From Figure 12(b), the sensitivity (absolute value) decreases as temperature increases. The main reason is that both lines are 'cold' lines with a similar low-state energy E''. Despite this, the line pair can satisfactorily infer temperatures over a wide range, as demonstrated by our experimental results below.

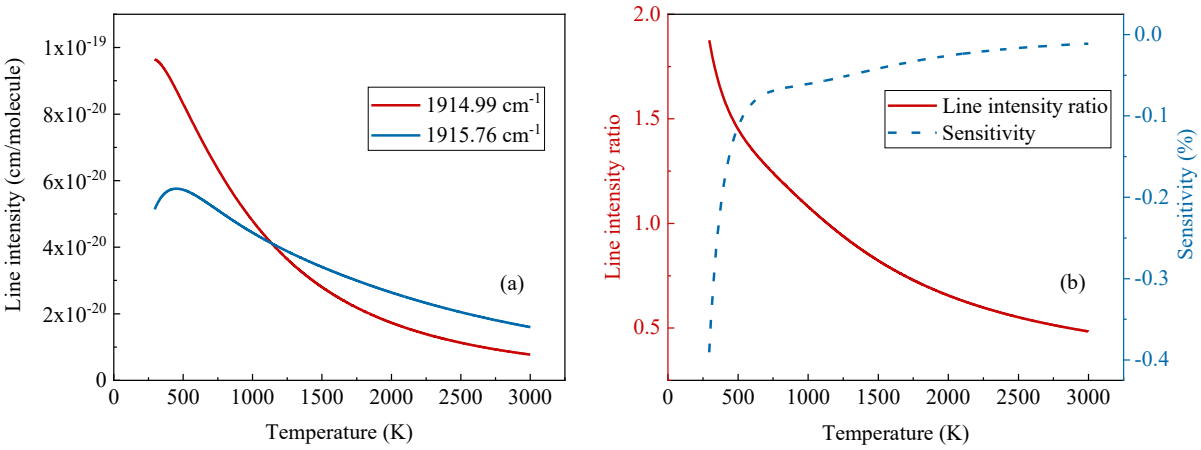

Figure 12. (a) Line intensity of two NO absorption peaks at 1914.99 cm^{-1} and 1915.76 cm^{-1} from 295-3000 K; (b) Line intensity ratio of line pair 1914.99 cm^{-1}/1915.76 cm^{-1} and temperature sensitivity between 295 and 3000 K

Using the same measurement cases in Figure 9, the dynamic temperatures at (T_1, P_1), (T_2, P_2) and (T_5, P_5) inferred by intrapulse laser are compared to the calculated temperature using one-dimensional shock equations, as shown in Figure 13. Overall, both sets of temperatures show good agreement over wide and dynamic temperature and pressure ranges. A linear regression was performed with the uncertainties in both the x-axis and y-axis taken into consideration. The correlation coefficient (Pearsons's r) is as high as 0.996. The average relative difference between the temperature inferred by the intrapulse laser and calculated temperature is 5.4%. The uncertainty in temperature inferred by intrapulse laser is 14.6%, mainly due to a 10% uncertainty in line intensity. Considering the potential for significant improvement in line intensity measurements, we assumed a 2% uncertainty in line intensity after careful

measurements. In this case, the uncertainty in temperature inferred by intrapulse laser can be reduced to 5.2%.

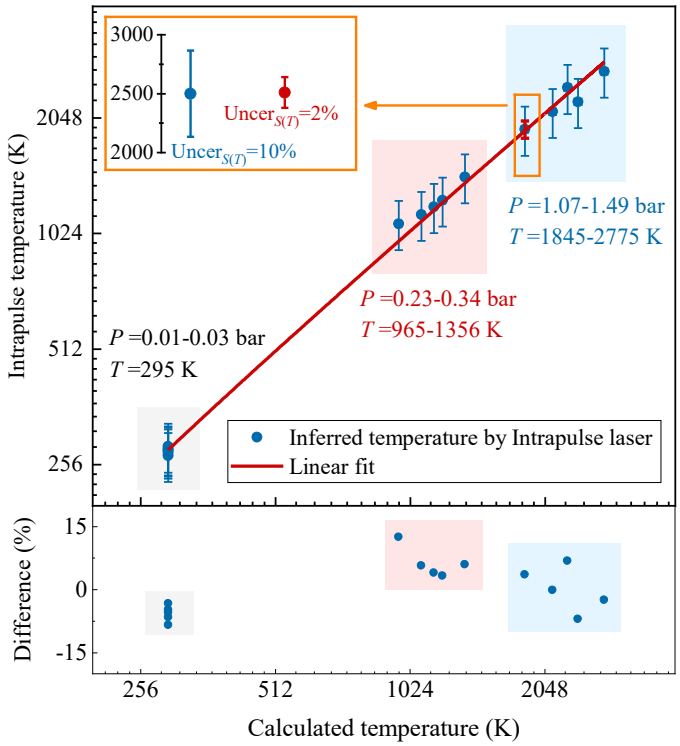

Figure 13. Linear fit between dynamic temperature measured by intrapulse laser and calculated temperature based on 1-D shock relations

To sum up, the capability of using intrapulse laser for dynamic NO, H_2O and temperature determination has been validated over wide pressure and temperature ranges using specific non-reactive mixtures. This is the basis for real applications as introduced below.

6. Application

This chapter demonstrates an application of using intrapulse laser for simultaneous dynamic measurement of NO, H_2O, and temperature during NH_3 oxidation in the shock tube. In recent years, facing an urgent situation in decarbonization, NH_3 is considered as a promising zero-carbon fuel. Through the electrolysis of water using renewable energy sources such as wind or solar power, the "green ammonia synthesis" enables the generation of ammonia without the emission of carbon dioxide. In our previous studies, we have studied the combustion chemistry of NH_3 fuel blends and developed a mechanism that can satisfactorily reproduce the experimental results [33]. Here, the mechanism is used to simulate speciation mole fractions and temperatures which will be compared with the results obtained from intrapulse laser. Besides, our previous studies [11,34] have observed strong adsorption effect of NH_3 and highlighted the importance of quantifying NH_3 mole fraction for shock tube experiments.

Hence, an independent QCL laser was used to determine the NH_3 mole fraction, which is an important input parameter for modelling.

Figure 14(a) shows a reference signal, transmitted signal, and absorbance of NO and H_2O spectrum at 2715 K and 1.21 bar during NH_3 oxidation in the shock tube. Two NO absorption peaks and two H_2O absorption peaks are clearly visible. The spectrum aligns well with simulation results shown previously in Figure 2. A multiple-peak Voigt fitting algorithm is used for spectrum simulation. The standard deviation of the fitting residual is 1.6×10^{-3}. Using the method described earlier, speciation mole fractions and dynamic temperature can be calculated from these spectra.

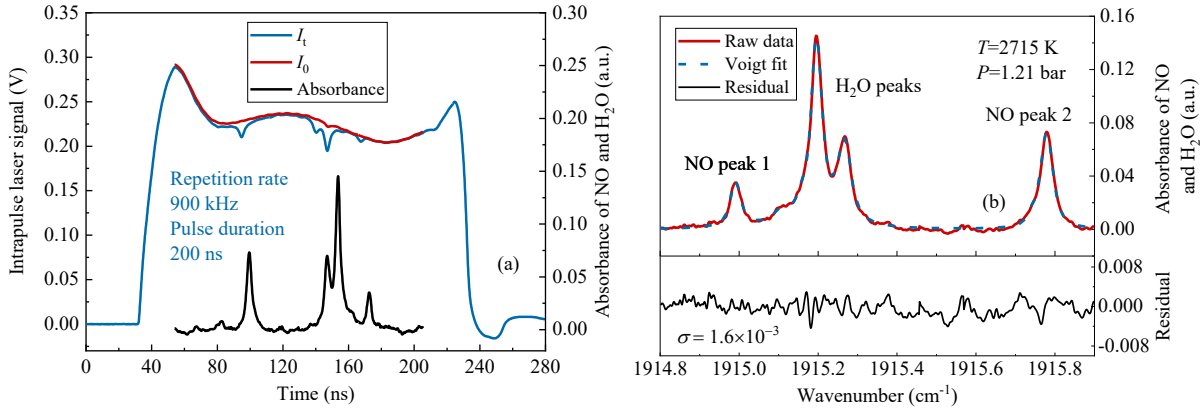

Figure 14. (a) Reference signal, transmitted signal, and absorbance of NO and H_2O spectrum during NH_3 oxidation in the shock tube; (b) Raw absorbance and Voigt fit of the NO and H_2O spectrum at 2715 K and 1.21 bar

Figure 15 depicts the time-resolved NO, H_2O and temperature measured by intrapulse laser in the shock tube with a mixture of 4% NH_3/6% O_2/90% Ar. The intrapulse laser effectively captures the formation process of NO and H_2O over time. Despite some fluctuations in the speciation profiles, there is generally good agreement between experimental and simulation results. As the dynamic temperature is inferred from the two NO absorption peaks, it only shows reasonable results after a certain time. Nevertheless, the dynamic temperature overall matches with the simulation results. This application case demonstrates that a single intrapulse laser can achieve simultaneous and dynamic measurement of multiple species and temperature with MHz time resolution, which combines the calibration-free nature of scanned-wavelength method with the high time resolution of fixed-wavelength method.

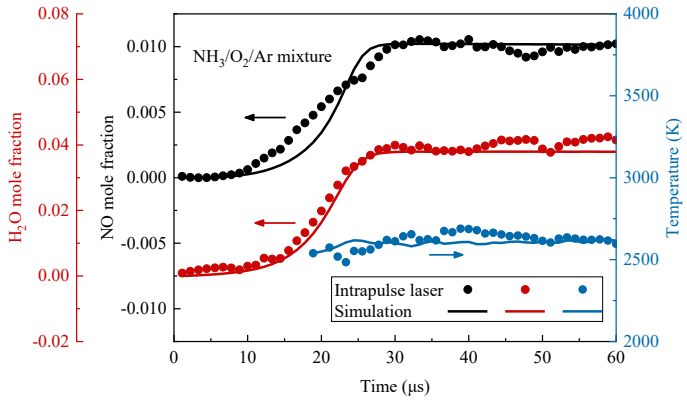

Figure 15. Time-resolved NO, H_2O and temperature measured by intrapulse laser in the shock tube with a mixture of 4% NH_3/6% O_2/90% Ar, and comparison to the simulation results

7. Conclusions

A shock tube serves as an ideal reactor for generating dynamic environments across a wide range of temperatures and pressures. The intrapulse laser technique is chosen to achieve simultaneous speciation mole fraction and temperature measurements couple to the shock tube. The fundamentals, validations, and applications of the intrapulse laser have been thoroughly investigated.

The spectral regions were selected ranging from 1914 to 1916 cm^{-1}, which covers distinct NO and H_2O absorption peaks for simultaneous measurements of NO and H_2O mole fraction as well as temperature through two-line thermometry. The intrapulse laser operated at a repetition rate of 900 kHz with a pulse width of 200 ns. The chirp rate of the intrapulse laser ranges from 250-400 MHz, corresponding to a spectral resolution of 0.0156 cm^{-1} to 0.0197 cm^{-1}. A strong rapid passage effect has been observed under low-pressure conditions. To correct the impact of the rapid passage effect on mole fraction calculations, we proposed a method by symmetrically flipping half of the spectrum that remains unaffected by the rapid passage effect. This method is relatively simple yet practical for applications. With this method, the relative difference between the NO mole fraction measured by the intrapulse laser and an ICL laser reduces from 10% to 1.3%.

The capability of the intrapulse laser in accurately quantifying NO mole fraction, H_2O mole fraction, and temperature has been validated through specifically designed experiments. The results show that both the NO and H_2O mole fractions aligned well with measurements obtained using an independent ICL NO laser and a DFB H_2O laser. The temperatures inferred by the intrapulse laser also show good agreement with temperatures calculated using one-dimensional shock equations with a correlation coefficient of 0.996. The average relative differences on NO

mole fraction, H_2O mole fraction and temperature are 4.5%, 7.0%, and 5.4%, respectively. Additionally, simultaneous dynamic measurement of NO, H_2O, and temperature using a single intrapulse laser has been demonstrated during NH_3 oxidation in the shock tube. The intrapulse laser can captured the formation process of NO and H_2O and temperature variation, showing generally good agreement with simulation results from a reaction mechanism.

This study has underscored that the intrapulse laser enables simultaneous and dynamic measurement of multiple species and temperatures with MHz time resolution, combining the scanned-wavelength method's calibration-free nature with the fixed-wavelength method's high time resolution.

Declaration of interests

None

Credit authorship contribution statement

Denghao Zhu: Conceptualization, Investigation, Visualization, Writing – original draft; **Leopold Seifert**: Investigation, Writing – review and editing; **Sumit Agarwal**: Investigation, Writing – review and editing; **Bo Shu**: Writing – review and editing; **Ravi Fernandes**: Writing – review and editing; **Zhechao Qu**: Conceptualization, Investigation, Writing – review and editing, Funding acquisition.

Acknowledgement

The project (Partnership project number and short name) has received funding from the European Partnership on Metrology, co-financed from the European Union's Horizon Europe Research and Innovation Programme and by the Participating States.

References

[1] A. Farooq, A.B.S. Alquaity, M. Raza, E.F. Nasir, S. Yao, W. Ren, Laser sensors for energy systems and process industries: Perspectives and directions, Prog. Energy Combust. Sci. 91 (2022) 100997.

[2] R.K. Hanson, R.M. Spearrin, C.S. Goldenstein, Spectroscopy and Optical Diagnostics for Gas, Switzerland: Springer International Publishing, 2016.

[3] J.D. Whitehead, I.D. Longley, M. W. Gallagher, Seasonal and Diurnal Variation in Atmospheric Ammonia in an Urban Environment Measured Using a Quantum Cascade Laser Absorption Spectrometer, Water Air Soil Pollut. 183 (2007) 317-329.

[4] A. Thompson, H. Northern, B. Williams, M. Hamilton, P. Ewart, Simultaneous detection of CO_2 and CO in engine exhaust using multi-mode absorption spectroscopy, MUMAS, Sens. Actuators B Chem. 198 (2014) 309-315.

[5] S. Barrass, Y. Gerard, R.J. Holdsworth, P.A. Martin, Near-infrared tunable diode laser spectrometer for the remote sensing of vehicle emissions, Spectrochim Acta A Mol Biomol Spectrosc 60 (2004) 3353-3360.

[6] A. Moriaux, R. Vallon, C. Cilindre, B. Parvitte, G. Liger-Belair, V. Zeninari, Development and validation of a diode laser sensor for gas-phase CO_2 monitoring above champagne and sparkling wines, Sens. Actuators B Chem. 257 (2018) 745-752.

[7] J. Li, C. Zhang, Y. Wei, Z. Du, F. Sun, Y. Ji, X. Yang, C. Liu, In situ, portable and robust laser sensor for simultaneous measurement of ammonia, water vapor and temperature in denitrification processes of coal fired power plants, Sens. Actuators B Chem. 305 (2020) 127533.

[8] K. Duan, Y. Ji, D. Wen, Z. Lu, K. Xu, W. Ren, Mid-infrared fiber-coupled laser absorption sensor for simultaneous NH_3 and NO monitoring in flue gases, Sens. Actuators B Chem. 374 (2023) 132805.

[9] M. Razeghi, Q.Y. Lu, N. Bandyopadhyay, W. Zhou, D. Heydari, Y. Bai, S. Slivken, Quantum cascade lasers: from tool to product, Opt. Express 23 (2015) 8462-8475.

[10] J. Li, U. Parchatka, H. Fischer, Development of field-deployable QCL sensor for simultaneous detection of ambient N_2O and CO, Sens. Actuators B Chem. 182 (2013) 659-667.

[11] D. Zhu, S. Agarwal, B. Shu, R. Fernandes, Z. Qu, An ultra-rapid optical gas standard for dynamic processes: Absolute NH_3 quantification and uncertainty evaluation, Measurement 230 (2024) 114559.

[12] E. Normand, M. McCulloch, G. Duxbury, and N. Langford, Fast, real-time spectrometer based on a pulsed quantum-cascade laser, Opt. Express 28 (2003) 16-18.

[13] J. Manne, W. Jäger, J. Tulip, Sensitive detection of ammonia and ethylene with a pulsed quantum cascade laser using intra and interpulse spectroscopic techniques, Appl. Phys. B 94 (2008) 337-344.

[14] J.A. Nwaboh, O. Werhahn, D. Schiel, Measurement of CO amount fractions using a pulsed quantum-cascade laser operated in the intrapulse mode, Appl. Phys. B 103 (2010) 947-957.

[15] C. Jacquemin, F. Defossez, R. Vallon, B. Parvitte, G. Maisons, M. Carras, V. Zeninari, Intrapulse measurement using a quantum cascade laser coupled with a compact dense

pattern multipass absorption cell for carbon dioxide monitoring, J. Opt. Soc. Am. B 40 (2022) 469404.

[16] F. Herklotz, T. Rubin, M. Sinnreich, A. Helmke, T. von Haimberger, K. Heyne, Fast Simultaneous CO_2 Gas Temperature and Concentration Measurements by Quantum Cascade Laser Absorption Spectroscopy, App. Sci. 12 (2022) 907045.

[17] F. Herklotz, T. Rubin, T. von Haimberger, K. Heyne, CO_2 Gas Temperature Sensing near Room Temperature by a Quantum Cascade Laser in Inter Pulse Mode, Photonics 9 (2022) 469404.

[18] M. Hübner, D. Marinov, O. Guaitella, A. Rousseau, J. Röpcke, On time resolved gas temperature measurements in a pulsed dc plasma using quantum cascade laser absorption spectroscopy, Meas. Sci. Technol. 23 (2012) 115602.

[19] R.S.M. Chrystie, E.F. Nasir, A. Farooq, Towards simultaneous calibration-free and ultra-fast sensing of temperature and species in the intrapulse mode, Proc. Combust. Inst. 35 (2015) 3757-3764.

[20] E.F. Nasir, A. Farooq, Time-resolved temperature measurements in a rapid compression machine using quantum cascade laser absorption in the intrapulse mode, Proc. Combust. Inst. 36 (2017) 4453-4460.

[21] E.F. Nasir, A. Farooq, Intra-pulse H2O absorption diagnostic for temperature sensing in a rapid compression machine, Appl. Phys. B 125 (2019) 210.

[22] G. Duxbury, N. Langford, M.T. McCulloch, S. Wright, Quantum cascade semiconductor infrared and far-infrared lasers: from trace gas sensing to non-linear optics, Chem Soc Rev 34 (2005) 921-934.

[23] G. Duxbury, N. Langford, M.T. McCulloch, S. Wright, Rapid passage induced population transfer and coherences in the 8 micron spectrum of nitrous oxide, Mol. Phys. 105 (2007) 741-754.

[24] G. Duxbury, N. Langford, K. Hay, Delayed rapid passage and transient gain signals generated using a chirped 8 μm quantum cascade laser, J. Mod. Opt. 55 (2008) 3293-3303.

[25] N. Tasinato, K.G. Hay, N. Langford, G. Duxbury, D. Wilson, Time dependent measurements of nitrous oxide and carbon dioxide collisional relaxation processes by a frequency down-chirped quantum cascade laser: rapid passage signals and the time dependence of collisional processes, J. Chem. Phys. 132 (2010) 164301.

[26] G. Duxbury, K. G. Hay, N. Langford, M.P. Johnson, J.D. Black, Real-time diagnostics of a jet engine exhaust using an intra-pulse quantum cascade laser spectrometer, Mol. Phys. 109 (2011) 17-18.

[27] J.H. van Helden, S.J. Horrocks, G.A.D. Ritchie, Application of quantum cascade lasers in studies of low-pressure plasmas: Characterization of rapid passage effects on density and temperature measurements, Appl. Phys. Lett. 92 (2008) 081506.

[28] D. Zhu, S. Agarwal, L. Seifert, B. Shu, R. Fernandes, Z. Qu, NH_3 absorption line study and application near 1084.6 cm^{-1}, Infrared Phys. Technol. 136 (2024) 105058.

[29] D. Zhu, Z. Qu, M. Li, S. Agarwal, R. Fernandes, B. Shu, Investigation on the NO formation of ammonia oxidation in a shock tube applying tunable diode laser absorption spectroscopy, Combust. Flame 246 (2022) 112389.

[30] S. Agarwal, L. Seifert, D. Zhu, B. Shu, R. Fernandes, Z. Qu, Investigations on Pressure Broadening Coefficients of NO Lines in the 1←0 Band for N_2, CO_2, Ar, H_2, O_2 and He, Appl. Sci. 13 (2023) 13031370.

[31] I. E. Gordon, L. S. Rothman, R. J. Hargreaves, R. Hashemi, E. V. Karlovets, F. M. Skinner, E. K. Conway, C. Hill, R. V. Kochanov and Y. Tan, et al., The HITRAN2020 molecular spectroscopic database, J. Quant. Spectrosc. Radiat. Transf. 277 (2022) 107949.

[32] JCGM 100:2008, Evaluation of measurement data — Guide to the expression of uncertainty in measurement, 2008

[33] M. Li, D. Zhu, H. Karas, S. Agarwal, Z. Qu, K. Moshammer, R. Fernandes, B. Shu, NH_3/C_2H_6 and NH_3/C_2H_5OH oxidation in a shock tube: Multi-speciation measurement, uncertainty analysis, and kinetic modeling, Chem. Eng. J., 2024 (under review).

[34] D. Zhu, L. Seifert, S. Agarwal, B. Shu, R. Fernandes, Z. Qu, NH_3 line broadening coefficients and intensities measurement and impurities determination in emerging applications: CCUS, Biomethane and H_2, Spectrochim Acta A Mol Biomol Spectrosc 320 (2024) 124642.